Magnetic anisotropy of two tetrahedral Co(II)-halide complexes with triphenylphosphine ligands

Wei Lv,[a] Hui-Hui Cui,[a] Lei Chen,[b] Yi-Quan Zhang,*[c] Xue-Tai Chen,*[a] Zhenxing Wang,*[d] Zhong-Wen Ouyang[d] and Zi-Ling Xue[e]

[a]*State Key Laboratory of Coordination Chemistry, School of Chemistry and Chemical Engineering, Nanjing University, Nanjing 210023, China*

[b]*School of Environmental and Chemical Engineering, Jiangsu University of Science and Technology, Zhenjiang 212003, China*

[c]*Jiangsu Key Laboratory for NSLSCS, School of Physical Science and Technology, Nanjing Normal University, Nanjing 210023, China*

[d]*Wuhan National High Magnetic Field Center & School of Physics, Huazhong University of Science and Technology, Wuhan 430074, China*

[e]*Department of Chemistry, University of Tennessee, Knoxville, Tennessee 37996, USA*

Electronic Supplementary Information

Table S1 Complexes with $[CoAB_3]$ moiety and their structure/magnetic parameters

Complex[a]	Coordination moiety	D/cm^{-1}	$\|E\|$/cm^{-1}	U_{eff} / K[b]	Reference
1	$[CoPCl_3]$	+42.8	0	c	This work
2	$[CoPBr_3]$	+41.2	0	c	This work
$[Co(L^1)Cl_3]$ (**3**)	$[CoNCl_3]$	+19.9	3.37	d	18
$[(L^2)CoCl]^+$ **(4)**	$[CoN_3Cl]$	+12.7	1.2	34.5 (1500 Oe)	19
$K[Co(L^3)]$ **(5)**	$[CoNN'_3]$	+33	0.2	45 (1000 Oe)	20
$[Co(L^4)]$ **(6)**	$[CoNN'_3]$	+16	0.0	12.5 (1500 Oe)	21
$[LiTHF][Co(L^5)]$ **(7)**	$[CoNN'_3]$	+27	4.0	26 (1000 Oe)	22

a. Ligands: L^1 = 2-methyl-3-(pyridin-2-yl)imidazo[1,5-a]pyridinium cation; $L^2 = CH_3C[CH_2N{=}CN(CH_3)_2]_3$; L^3 = N,N',N''-[nitrilotris-(ethane-2,1-diyl)]tris(2,4,6-trimethylbenzenesulfonamide); $L^4 = N[CH_2C(O)NC(CH_3)_3]_3$; $L^5 = [(Me_3SiNCH_2CH_2)_3N]^{3-}$. b. The applied field used in the measurement is indicated in the parenthesis. c. No Orbach mechanism is found. d. Not reported.

Table S2 Complexes with $[CoP_2X_2]$ moiety and their structure/magnetic parameters

Complex	Coordination moiety	D /cm^{-1}	$\|E\|$ /cm^{-1}	U_{eff} / K[c]	Reference
$[Co(PPh_3)_2Cl_2]$ **(8)**	$[CoP_2Cl_2]$	-16.2	0.9	37.1 (1000 Oe)	23
$[Co(L^6)Cl_2]$ **(9)**	$[CoP_2Cl_2]$	-14.4	1.7	35.0 (1000 Oe)	23
$[Co(L^7)Cl_2]$ **(10)**	$[CoP_2Cl_2]$	-15.4	1.3	29.9 (1000 Oe)	23
$[Co(PPh_3)_2Br_2]$ **(11)**	$[CoP_2Br_2]$	-13	--	37 (1000 Oe)	24
$[Co(PPh_3)_2I_2]$ (**12**)	$[CoP_2I_2]$	-36.9	0.2	30.6 (1000 Oe)	25
$[Co(PPh_3)_2(NCS)_2]$(**13**)	$[CoP_2N_2]$	-9.44	1.60	b	26
$[Co(L^8)(NCS)_2]$ **(14)**	$[CoP_2N_2]$	-11.4	0.46	31.8 (3000 Oe)	27
$[Co(L^9)(NCS)_2]$ **(15)**	$[CoP_2N_2]$	-16.2	1.1	30.1 (1000 Oe)	28
$[Co(L^9)Cl_2]$ **(16)**	$[CoP_2Cl_2]$	-15.1	0.9	25.5 (1000 Oe)	28
$[Co(L^9)Br_2]$ **(17)**	$[CoP_2Br_2]$	-11.6	1.2	18.7 (1000 Oe)	28
$[Co(L^9)I_2]$ **(18)**	$[CoP_2I_2]$	-7.3	1.5	9.2 (1000 Oe)	28
$[CoCl_2(dppf)]$ **(19)**	$[CoP_2Cl_2]$	-11.0	0	33.3 (1000 Oe)	29
$[CoBr_2(dppf)]$ **(20)**	$[CoP_2Br_2]$	-8.7	2.09	28.8 (1000 Oe)	29

a. Ligands: L^6 = DPEphos = 2,2'-bis(diphenyl-phosphino) diphenyl ether; L^7 = Xantphos = 9,9-dimethyl-4,5-bis(diphenyl-phosphino) xanthenes; L^8 = bis(2-(diphenylphosphaneyl)-4-methylphenyl)amine; L^9 = 9,9-dimethyl-4,5-bis(diphenylphosphino)xanthenes; dppf = 1,1′-ferrocenediyl-bis(diphenylphosphine). b. Not reported. c. The applied field used in the measurement is indicated in the parenthesis.

Table S3 Summary of crystal data and refinement for **1** and **2**

	1	**2**
Molecular formula	$C_{26}H_{35}NPCl_3Co$	$C_{26}H_{35}NPBr_3Co$
CCDC no	2074688	2074732
Formula weight	557.80	691.18
Temperature/K	296(2)	296(2)
Crystal system	Cubic	Cubic
Space group	*Pa*	*Pa*
a / Å	17.5892(2)	17.86950(10)
b / Å	17.5892(2)	17.86950(10)
c / Å	17.5892(2)	17.86950(10)
α (°)	90	90
β (°)	90	90
γ (°)	90	90
V / Å^3	5441.75(19)	5706.17(10)
Z	8	8
D_{calc}, g/cm^3	1.362	1.609
μ / mm^{-1}	0.999	4.873
F (000)	2328.0	2760.0
θ range [°]	2.005/25.977	1.974/25.974
Reflns collected	42768	45367
R_{int}	0.0574	0.0608
Indep. reflns	1795	1869
Data/restr./paras	1795/215/149	1869/203/149
Goodness-of-fit on F^2	1.064	1.094
R_1, wR_2 [I > 2σ(*I*)][a]	0.0600/0.1565	0.0750/0.1755
R_1, wR_2 [all data][a]	0.0740/0.1700	0.0946/0.1889

[a]$wR_2 = [\Sigma[w(F_o^2–F_c^2)^2]/\Sigma[w(Fo^2)^2]]^{1/2}$, $R_1 = \Sigma||F_o|–|F_c||/\Sigma|F_o|$.

Table S4 Selected bond lengths (Angstroms) and angels (degree) for **1** and **2**

1		**2**	
Co1-P1	2.3763(16)	Co1-P1	2.373(3)
Co1-Cl1	2.2508(12)	Co1-Br1	2.3827(10)
Cl1-Co1-Cl1	114.11(4)	Br1-Co1-Br1	113.39(4)
P1-Co1-Cl1	104.30(5)	P1-Co1-Br1	105.19(5)

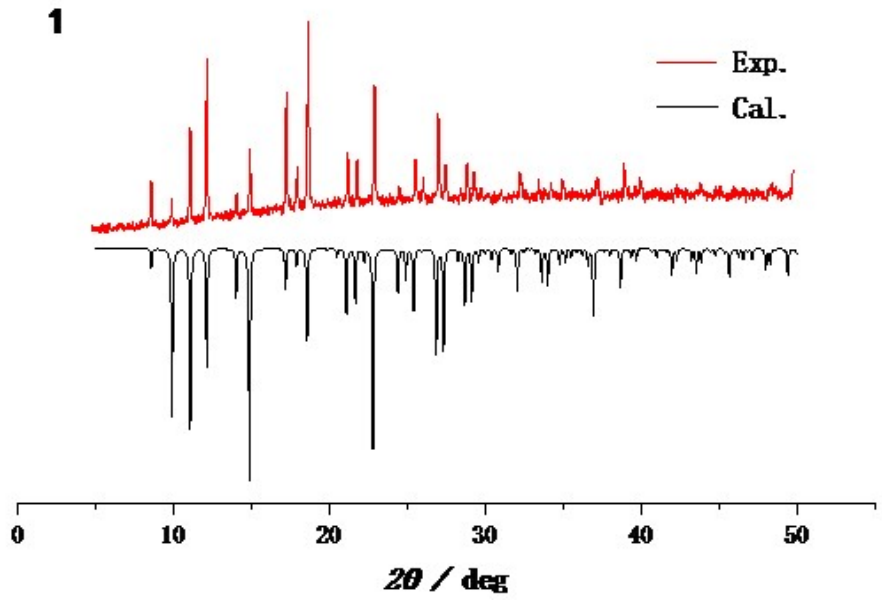

Fig. S1 XRD patterns for **1** (The red line are PXRD experimental pattern and the black line are calculated from single-crystal structure)

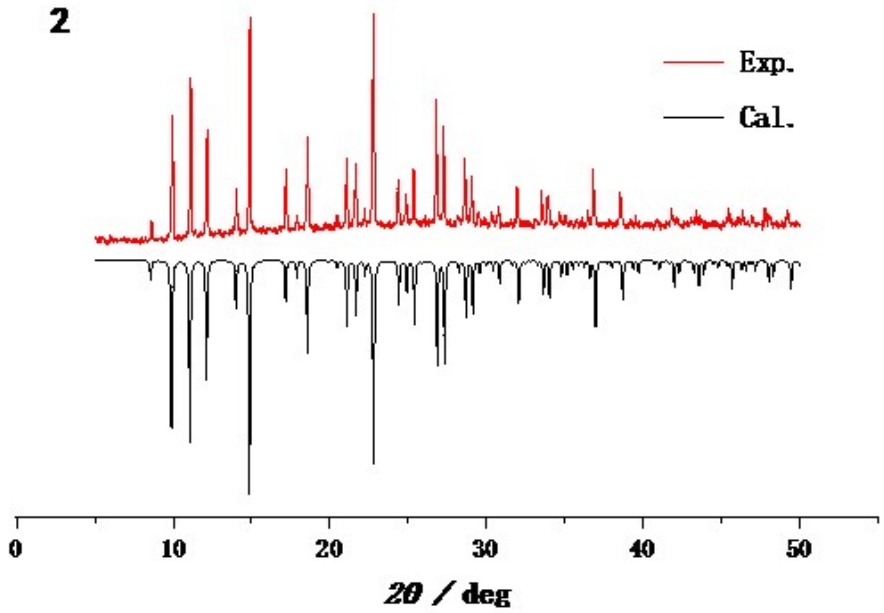

Fig. S2 XRD patterns for complex **2** (The red line are PXRD experimental pattern and the black line are calculated from single-crystal structure).

Table S4 The results of the continuous shape measure (*CShM*) analyses of **1** and **2** by SHAPE software.[1, 2]

Four-vertex	Deviation parameter			
	Square	Tetrahedron	Seesaw	Vacant trigonal bipyramid
1	33.432	0.177	8.903	2.258
2	33.417	0.199	8.889	2.112

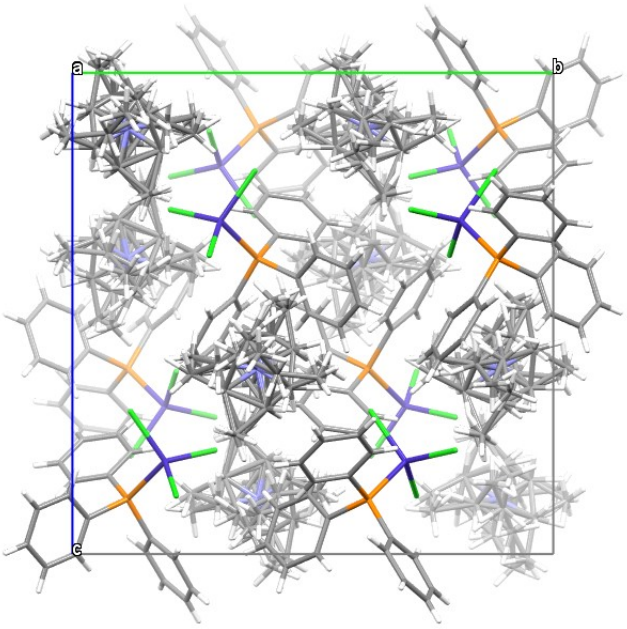

Fig. S3 Crsytal packing of **1** along the crystallographic a-axis.

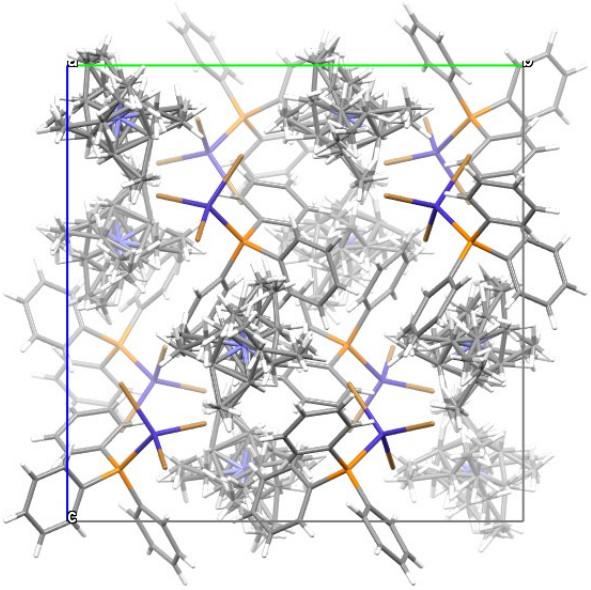

Fig. S4 Crystal packing of **2** along the crystallographic a-axis.

PHI survey plots: In oder to check the accuracy of the set of the fitted parameters, survey features have been performed using the PHI code.[3] Among the three parameters D, $g_x(g_y)$ and g_z, one parameter was fixed and the other two are varied. All the survey plots show that the fitted parameters are in the narrow minimum regions.

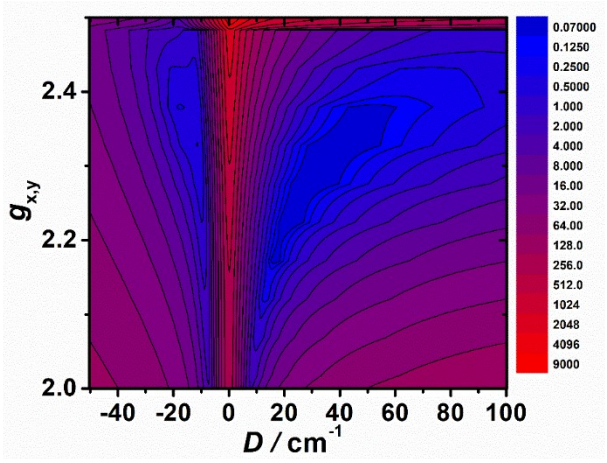

(a)

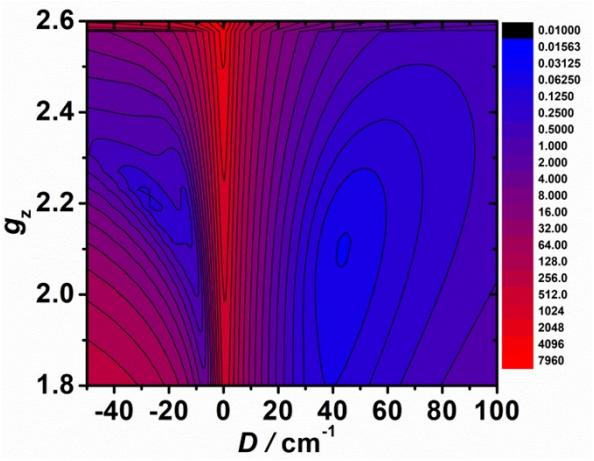

(b)

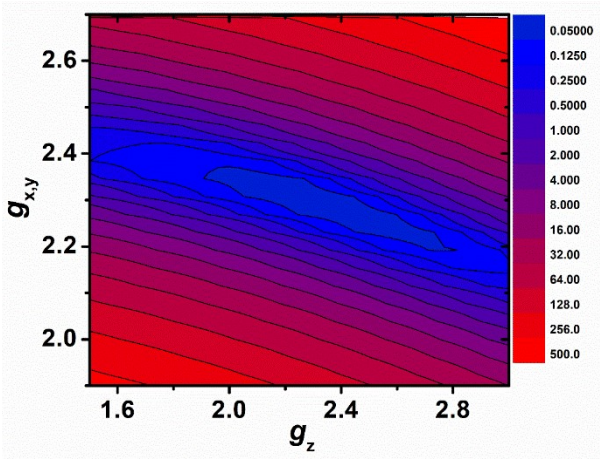

(c)

Fig. S5 The survey plots of complex **1**: (a) g_z was fixed as 2.103; (b) $g_x(g_y)$ was fixed as 2.236 and (c) D was fixed as 42.8 cm^{-1}.

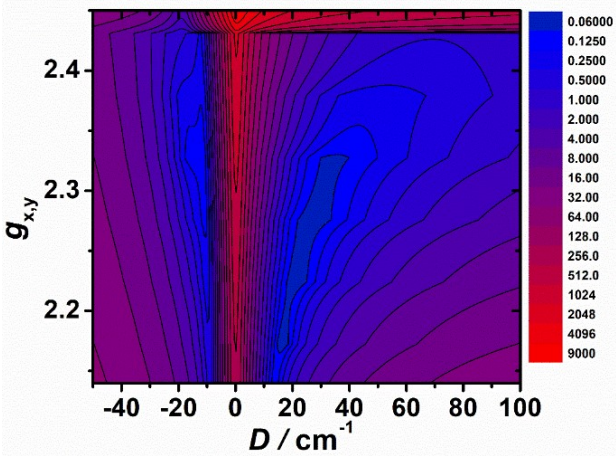

(a)

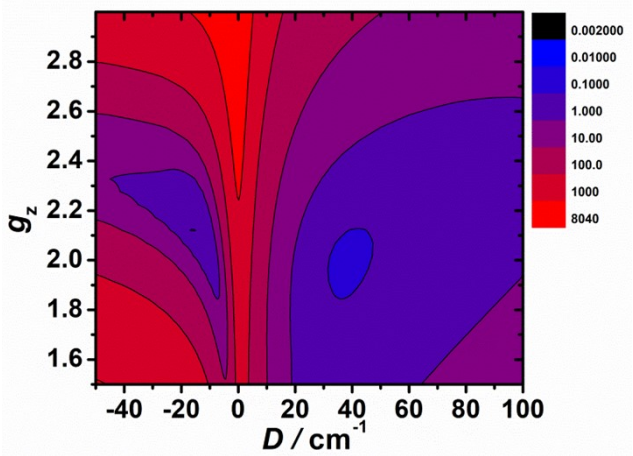

(b)

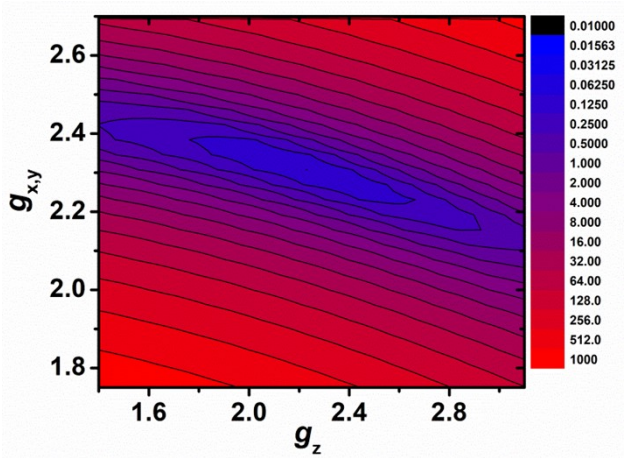

(c)

Fig. S6 The survey plots of complex **2**: (a) g_z was fixed as 2.136; (b) $g_x(g_y)$ was fixed as 2.262 and (c) D was fixed as 41.2 cm^{-1}.

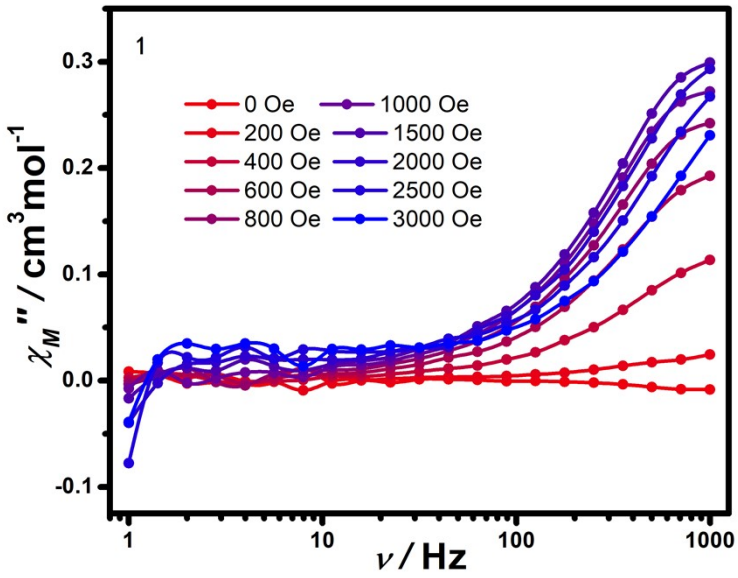

(a)

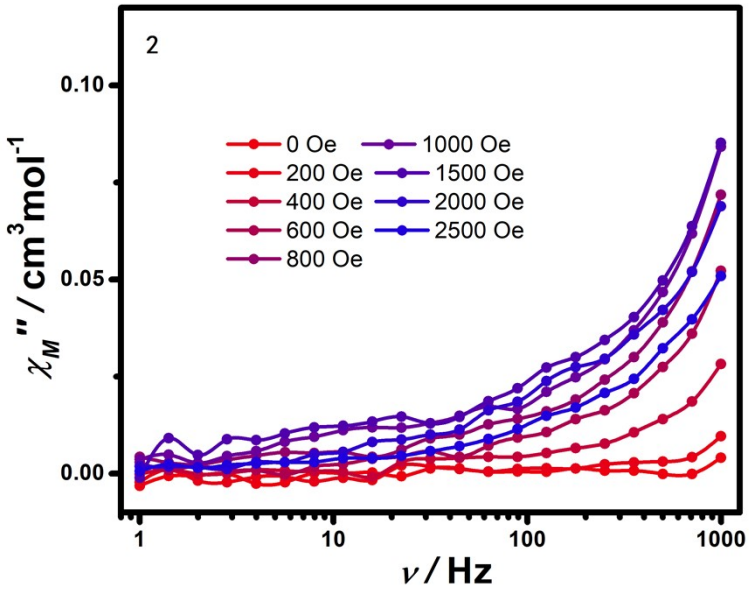

(b)

Fig. S7 Frequency dependence of out-of-phase ac susceptibility (χ_M'') at 1.8 K under the different applied static fields from 0 to 0.25 T for **1** (a) and **2** (b). The solid lines are for eye guide.

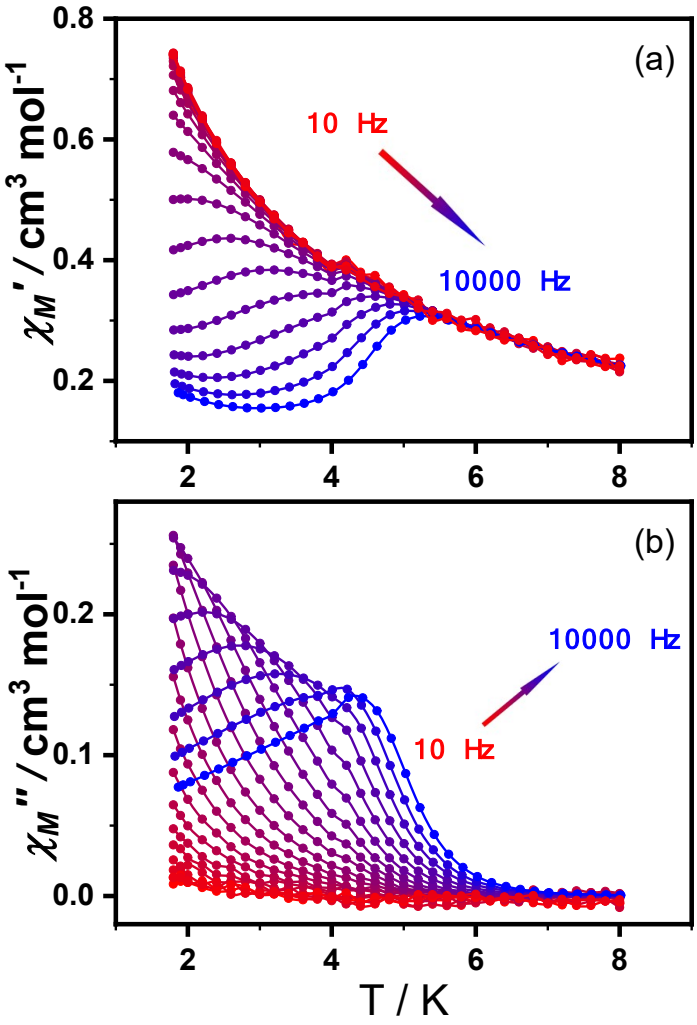

Fig. S8 Temperature dependence of (a) in-phase (χ_M') and (b) out-of-phase ac susceptibility (χ_M'') at different ac frequencies under the dc field of 0.12 T for **1**. The solid lines are for eye guide.

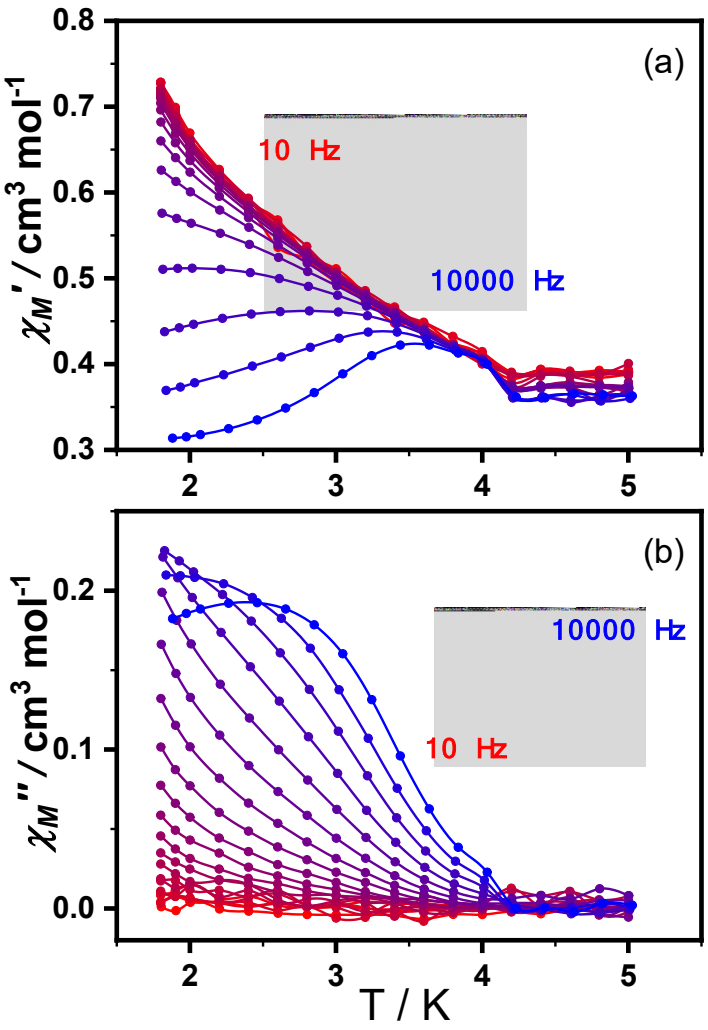

Fig. S9 Temperature dependence of (a) in-phase (χ_M') and (b) out-of-phase ac susceptibility (χ_M'') at different ac frequencies under the dc field of 0.15 T for **2**. The solid lines are for eye guide.

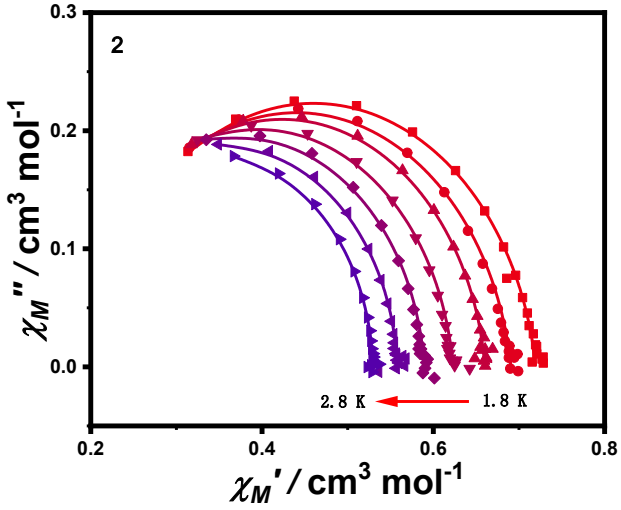

Fig. S10 Cole−Cole plots for **2** under 0.15 T dc field. The solid lines are the best fits to the experiments with the generalized Debye model.

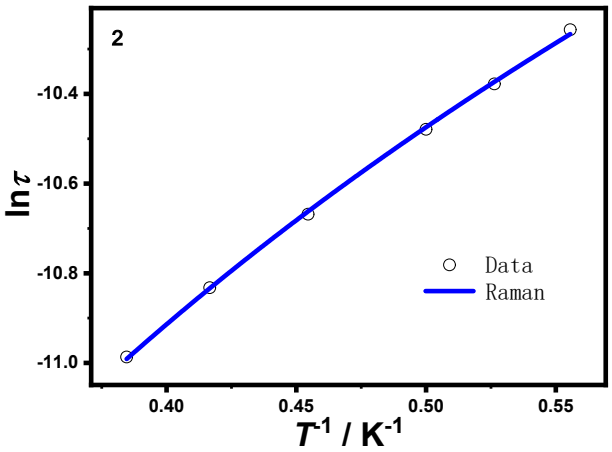

Fig. S11 The plot of ln(τ) versus T^{-1} for **2**. The solid blue line represents the best fit by the Raman process.

Table S5 Relaxation times τ (s) and α values for **1** and **2**

1				
T (K)	χ_S	χ_T	τ (s)	α
1.8	0.16775	0.7448	1.46616×10^{-4}	0.07053
1.9	0.16128	0.71303	1.33689×10^{-4}	0.0677
2.0	0.1559	0.68453	1.22337×10^{-4}	0.0625
2.2	0.15031	0.66035	1.1247×10^{-4}	0.06088
2.4	0.14531	0.63827	1.03745×10^{-4}	0.05875
2.6	0.14109	0.61614	9.56154×10^{-5}	0.05418
2.8	0.13704	0.5963	8.83302×10^{-5}	0.05117
3.0	0.13348	0.57683	8.16139×10^{-5}	0.04658
3.2	0.12929	0.55981	7.55874×10^{-5}	0.04619
3.4	0.1259	0.5438	7.01833×10^{-5}	0.04433
3.6	0.12413	0.52708	6.51943×10^{-5}	0.03701
3.8	0.12039	0.51323	6.06515×10^{-5}	0.03822
4.0	0.11787	0.49878	5.6357×10^{-5}	0.03462
4.4	0.11575	0.48508	5.2464×10^{-5}	0.03065
4.8	0.11296	0.47285	4.88591×10^{-5}	0.03029
5.2	0.11133	0.45994	4.54591×10^{-5}	0.02472
5.6	0.10949	0.44831	4.23382×10^{-5}	0.02156
6.0	0.10701	0.43822	3.93648×10^{-5}	0.02217
6.4	0.10504	0.42854	3.65816×10^{-5}	0.02144
6.8	0.1026	0.4181	3.37456×10^{-5}	0.01988
7.2	0.1023	0.40843	3.12653×10^{-5}	0.01367
7.6	0.1009	0.39929	2.87198×10^{-5}	0.01058
8.0	0.09871	0.39092	2.61773×10^{-5}	0.01048
2				
T (K)	χ_S	χ_T	τ (s)	α

1.8	0.20105	0.71947	3.51115×10^{-5}	0.08591
1.9	0.18959	0.6906	3.11135×10^{-5}	0.08737
2.0	0.18673	0.66015	2.81235×10^{-5}	0.06759
2.2	0.16967	0.62287	2.32724×10^{-5}	0.06667
2.4	0.16144	0.58927	1.97552×10^{-5}	0.05378
2.6	0.15936	0.5578	1.69242×10^{-5}	0.03441
2.8	0.15789	0.52916	1.41798×10^{-5}	0.01963
3.0	0.14601	0.50458	1.08899×10^{-5}	0.02683
3.2	0.14768	0.48031	8.20644×10^{-6}	0.01659
3.4	0.16043	0.45787	6.05389×10^{-6}	8.27505×10^{-4}
3.6	0.22726	0.44122	5.30153×10^{-6}	0.00112
4.0	0.00937	0.4237	1.14426×10^{-6}	0.11771
4.2	1.98419×10^{-7}	0.40805	3.95027×10^{-7}	0.23328
4.4	3.04973×10^{-7}	0.39081	1.97231×10-7	0.24095
4.6	1.94707×10^{-6}	0.37507	1.37693×10^{-7}	0.19865
4.8	9.15375×10^{-6}	0.36211	2.40381×10^{-8}	0.34942
5.0	1.77633×10^{-5}	0.34628	1.55948×10^{-7}	7.46318×10^{-9}

Compoutation Details

Complete active space second-order multiconfigurational perturbation theory (CASPT2) considering the effect of the dynamic electron correlation with MOLCAS 8.4 program package[4] was performed on the basis of single-crystal X-ray determined geometries of **1** and **2** (see Fig. S8 for the calculated model structures of **1** and **2**).

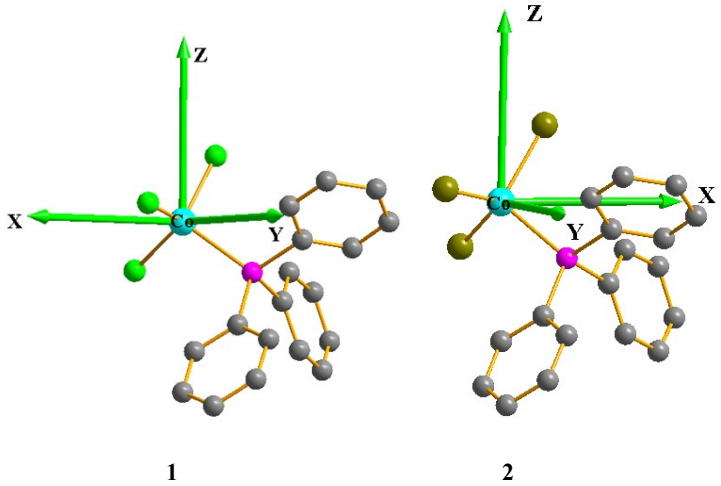

Fig. S12 Calculated model structures of individual Co^{II} fragments. H atoms are omitted for clarity.

For the first complete-active-space self-consistent field (CASSCF) calculation, the basis sets for all atoms are atomic natural orbitals from the MOLCAS ANO-RCC library: ANO-RCC-VTZP for magnetic center ion Co^{II}; VTZ for close Br, Cl and P atoms; VDZ for distant atoms. The calculations employed the second order Douglas-Kroll-Hess Hamiltonian, where scalar relativistic contractions were taken into account in the basis set. The active electrons in 5+5′ active orbitals include all d electrons (CAS(7 in 5+5′)) in the CASSCF calculations. To exclude all the doubts, we calculated all the roots in the active orbitals. The effect of the dynamical electronic correlation was applied using CASPT2 based on the first CASSCF calculation. After that, the spin-orbit coupling was handled separately in the restricted active space state interaction (RASSI-SO)

procedure.[5, 6] We have mixed the maximum number of spin-free state which was possible with our hardware (all from 10 quadruplets and 40 doublets). SINGLE_ANISO[7-9] program was used to obtain zero-field splitting parameters D (E) (cm^{-1}), $\boldsymbol{g}$ tensors, energy levels, magnetic axes, *et al.* based on the above CASPT2/RASSI-SO calculations.

To deeply analyze the magnetic anisotropy, ORCA 4.2 calculations[10] were performed with CASSCF, followed by N-electron valence second-order perturbation theory (NEVPT2). The spin-orbit coupling (SOC) operator used was the efficient implementation of the multicenter spin-orbit mean-field (SOMF) concept developed by Hess et al.[6] The spin-spin contributions (SSC) to the D values were also included although they are very small for our complexes. The NEVPT2[11-14] calculation with seven 3d electrons in five Co 3d-based orbitals (CAS(7, 5)). In the calculations, the orbitals were determined for the average of 10 $S = 3/2$ and 40 $S = 1/2$ roots. All calculations were performed with triple-ζ with one polarization function def2-TZVP[15-17] basis set for all atoms.

Table S6 Calculated spin-free energies (cm^{-1}) of the lowest ten terms (S = 3/2) of **1** and **2** using CASPT2/RASSI-SO with MOLCAS 8.4.

spin-free states	**1**	**2**
	E/cm^{-1}	E/cm^{-1}
1	0.0	0.0
2	2817.1	2684.3
3	3209.6	3174.9
4	3616.5	3290.2
5	4091.9	3654.0
6	8444.8	7742.8
7	8446.9	7747.4
8	16389.8	16959.3
9	16403.9	16994.2
10	19328.5	18823.7

Table S7 Calculated weights of the five most important spin-orbit-free states for the lowest two spin-orbit states of **1** and **2** using CASPT2/RASSI-SO with MOLCAS 8.4.

	Spin-orbit states	Energy (cm^{-1})	Spin-free states, Spin, Weights				
1	1	0.0	1,1.5,0.9580	3,1.5,0.0171	4,1.5,0.0106	2,1.5,0.0102	5,1.5,0.0019
	2	78.2	1,1.5,0.9728	3,1.5,0.0091	2,1.5,0.0084	4,1.5,0.0073	5,1.5,0.0013
2	1	0.0	1,1.5,0.9580	3,1.5,0.0178	4,1.5,0.0166	2,1.5,0.0038	5,1.5,0.0019
	2	63.6	1,1.5,0.9690	2,1.5,0.0101	4,1.5,0.0096	3,1.5,0.0089	5,1.5,0.0012

Table S8 Contributions of the excited states (with relative energy cm^{-1}) to *D* and *E* values (cm^{-1}) for **1** and **2** using NEVPT2 with ORCA 4.2.

Fragments	State No.	Mult	Energy, cm^{-1}	Contribution, cm^{-1}	Contribution, cm^{-1}
				D	*E*
1	1	4	2923.4	–10.039	0.000
	2	4	2972.8	16.636	15.973
	3	4	2974.4	16.618	–15.973
2	1	4	2384.2	–12.687	0.000
	2	4	2705.1	16.733	16.629
	3	4	2707.0	16.718	–16.629

Table S9 Relative energies (cm^{-1}) of ligand field one-electron states (in the basis of d-AOs) of **1** and **2** from AILFT analysis using NEVPT2 with ORCA 4.2.

Fragments	No.	LF one-electron state	Energy, cm^{-1}
1	1	$0.97\ d_{yz} - 0.15\ d_{xy} - 0.15\ d_{x2-y2}$	0.0
	2	$0.97\ d_{xz} - 0.16\ d_{xy} + 0.15\ d_{x2-y2}$	2.1
	3	$0.94\ d_{xy} + 0.27\ d_{x2-y2}$	3761.4
	4	$-0.94\ d_{x2-y2} + 0.27\ d_{xy}$	3763.9
	5	$1.00\ d_{z2}$	3933.5
2	1	$-0.97\ d_{yz} - 0.24\ d_{x2-y2}$	0.0
	2	$0.97\ d_{xz} + 0.24\ d_{xy}$	1.9
	3	$0.95\ d_{xy} - 0.23\ d_{xz}$	3094.6
	4	$0.95\ d_{x2-y2} - 0.23\ d_{yz}$	3096.5
	5	$1.00\ d_{z2}$	3929.6

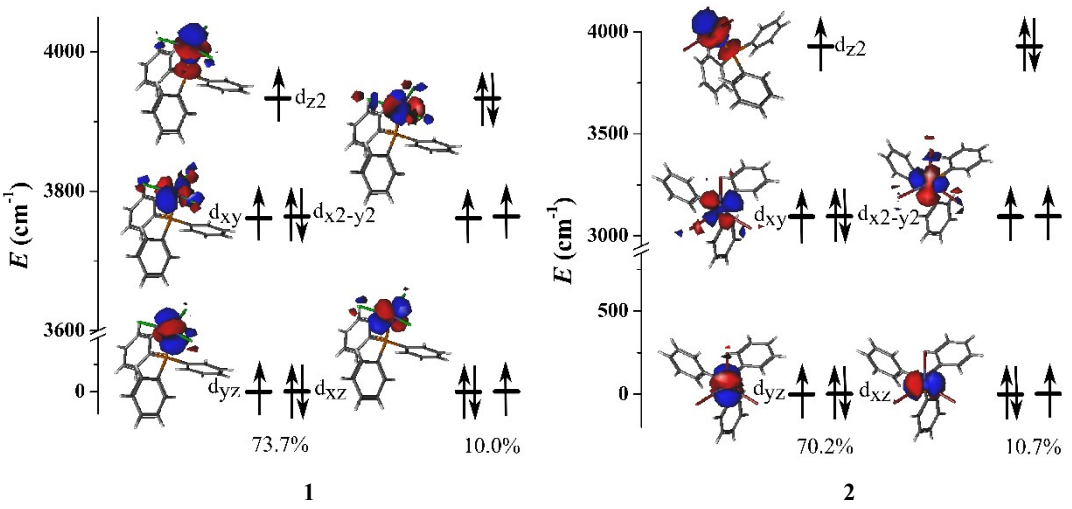

Fig. S13 Orbital energies computed for the ground states of **1** and **2** using NEVPT2 with ORCA 4.2. The percentage mention reveals the percent of the corresponding configuration mixing.

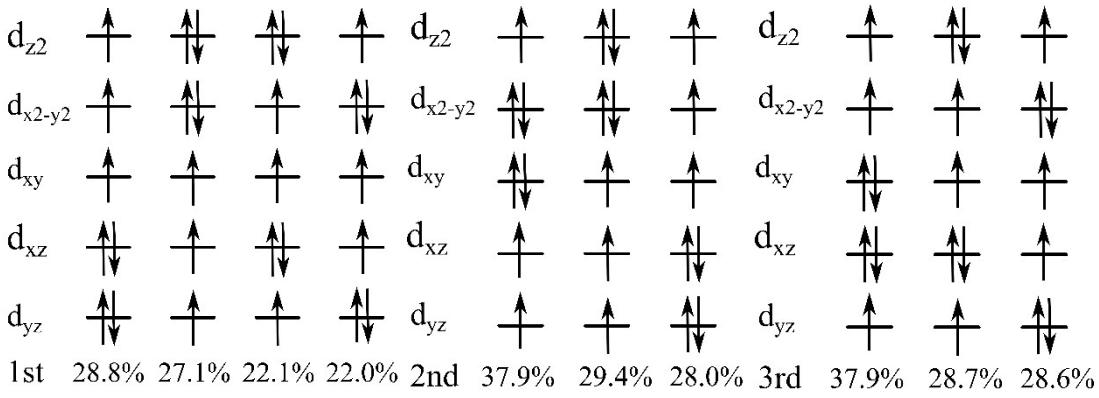

1

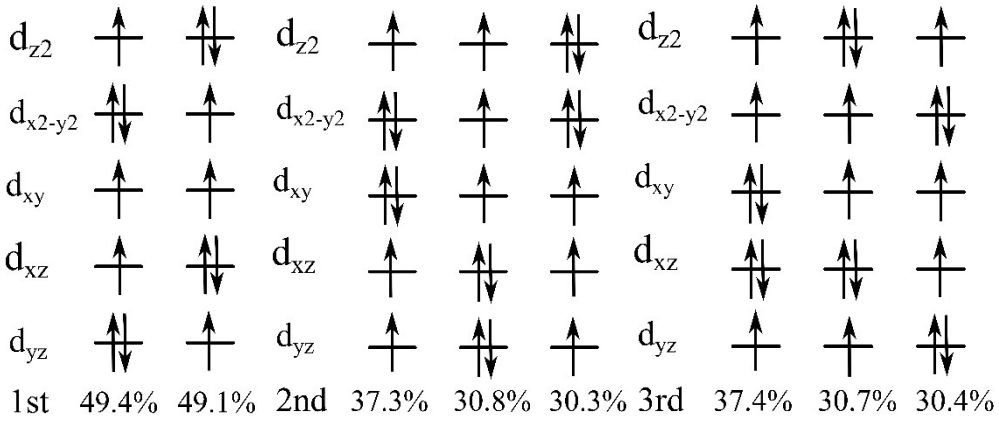

2

Fig. S14 Multi-determinant wavefunction of the selected excited states having important contributions to *D* tensor for **1** and **2**. The computed CI coefficients that are larger than 10% are shown above.

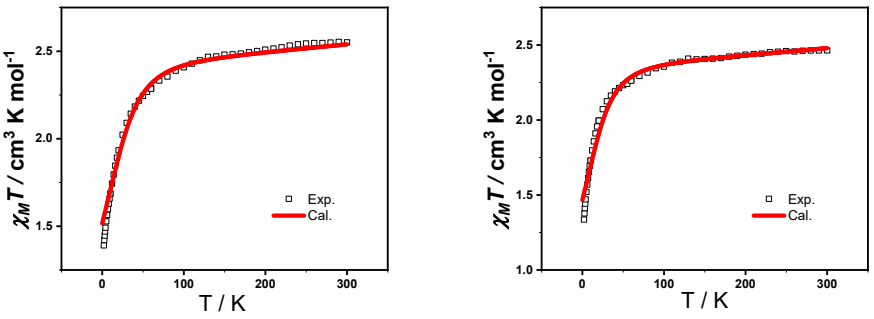

Fig. S15 Comparisons of the calculated (solid line) and the experimental magnetic susceptibilities for **1**–**2**.

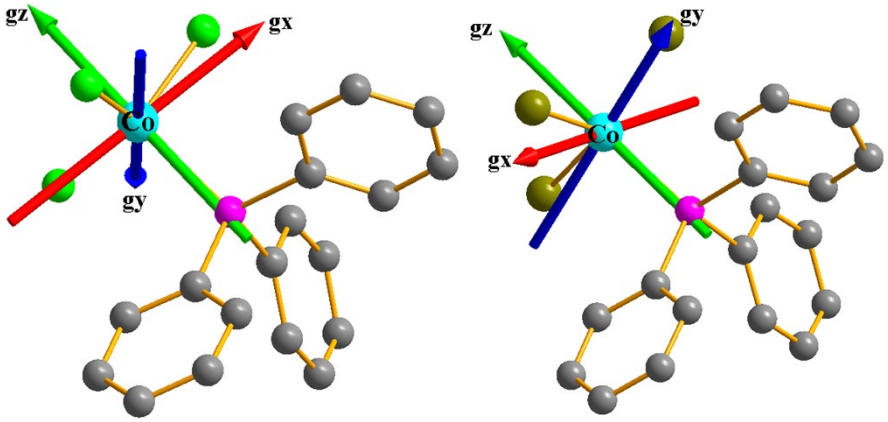

Fig. S16 Orientations of the local magnetic axes (red: g_x; blue: g_y; green: g_z) on Co^{II} ions of **1** and **2** in their ground spin-orbit states using CASPT2/RASSI-SO with MOLCAS 8.4.

Notes and references

1. M. Llunell, D. Casanova, J. Cirera, P. Alemany and S. Alvarez, *Shape Program Vision 2.1,* 2013.
2. S. Alvarez, P. Alemany, D. Casanova, J. Cirera, M. Llunell and D. Avnir, *Coord. Chem. Rev.*, 2005, **249**, 1693-1708.
3. N. F. Chilton, R, P. Anderson, L. D. Turner, A. Soncini and K. S. Murray, *J. Comput. Chem.*, 2013, **34**, 1164-75.
4. F. Aquilante, J. Autschbach, R. K. Carlson, L. F. Chibotaru, M. G. Delcey, L. De Vico, I. Fdez Galván, N. Ferré, L. M. Frutos, L. Gagliardi, M. Garavelli, A. Giussani, C. E. Hoyer, G. Li Manni, H. Lischka, D. Ma, P. Malmqvist, T. Müller, A. Nenov, M. Olivucci, T. B. Pedersen, D. Peng, F. Plasser, B. Pritchard, M. Reiher, I. Rivalta, I. Schapiro, J. Segarra-Martí, M. Stenrup, D. G. Truhlar, L. Ungur, A. Valentini, S. Vancoillie, V. Veryazov, V. P. Vysotskiy, O. Weingart, F. Zapata and R. Lindh, *J. Comput. Chem.*, 2016, **37**, 506-541.
5. P. Å. Malmqvist, B. O. Roos and B. Schimmelpfennig, *Chem. Phys. Letters*, 2002, **357**, 230–240.
6. B. A. Heß, C. M. Marian, U. Wahlgren and O. Gropen, *Chem. Phys. Letters*, 1996, **251**, 365-371.
7. L. F. Chibotaru, L. Ungur and A. Soncini, *Angew. Chem. Int. Ed.*, 2008, **47**, 4126-4129.
8. L. Ungur, W. Van den Heuvel and L. F. Chibotaru, *New J. Chem.*, 2009, **33**, 1224-1230.
9. L. F. Chibotaru, L. Ungur, C. Aronica, H. Elmoll, G. Pilet and D. Luneau, *J. Am. Chem. Soc.*, 2008, **130**, 12445-12455.
10. F. Neese, *Max-Plank institute for bioinorganic chemistr,* Mülheim an der Ruhr, Germany, 2019.
11. C. Angeli, R. Cimiraglia and J. P. Malrieu, *J. Chem. Phys.*, 2002, **117**, 9138-9153.
12. C. Angeli, R. Cimiraglia and J.-P. Malrieu, *Chem. Phys. Letters*, 2001, **350**, 297-305.
13. C. Angeli and R. Cimiraglia, *Theor. Chem. Acc.*, 2002, **107**, 313-317.
14. C. Angeli, R. Cimiraglia, S. Evangelisti, T. Leininger and J. P. Malrieu, *J. Chem. Phys.*, 2001, **114**, 10252-10264.
15. A. Schäfer, C. Huber and R. Ahlrichs, *J. Chem. Phys.*, 1994, **100**, 5829-5835.
16. A. Schäfer, H. Horn and R. Ahlrichs, *J. Chem. Phys*, 1992, **97**, 2571-2577.

17. F. Weigend and R. Ahlrichs, *Phys. Chem. Chem. Phys.*, 2005, **7**, 3297-3305.

18. O. Y. Vassilyeva, E. A. Buvaylo, V. N. Kokozay, B. W. Skelton, C. Rajnak, J. Titis and R. Boca, *Dalton Trans*, 2019, **48**, 11278-11284.

19. J. M. Zadrozny, J. Liu, N. A. Piro, C. J. Chang, S. Hill and J. R. Long, *Chem. Commun.*, 2012, **48**, 3927-3929.

20. K. A. Schulte, K. R. Vignesh and K. R. Dunbar, *Chem. Sci.*, 2018, **9**, 9018-9026.

21. S. Gomez-Coca, E. Cremades, N. Aliaga-Alcalde and E. Ruiz, *J. Am. Chem. Soc.*, 2013, **135**, 7010-7018.

22. D. Pinkowicz, F. J. Birk, M. Magott, K. Schulte and K. R. Dunbar, *Chem. Eur, J.*, 2017, **23**, 3548-3552.

23. F. Yang, Q. Zhou, Y. Zhang, G. Zeng, G. Li, Z. Shi, B. Wang and S. Feng, *Chem Commun*, 2013, **49**, 5289-91.

24. R. Boča, J. Miklovič and J. Titiš, *Inorg. Chem.*, 2014, **53**, 2367-2369.

25. M. R. Saber and K. R. Dunbar, *Chem Commun*, 2014, **50**, 12266-9.

26. C. Rajnák, A. Packová, J. Titiš, J. Miklovič, J. Moncol' and R. Boča, *Polyhedron*, 2016, **110**, 85-92.

27. Y.-Q. Zhai, Y.-F. Deng and Y.-Z. Zheng, *Dalton Trans.*, 2018, **47**, 8874-8878.

28. A. K. Mondal, M. Sundararajan and S. Konar, *Dalton Trans*, 2018, **47**, 3745-3754.

29. J. Hruby, D. Dvorak, L. Squillantini, M. Mannini, J. van Slageren, R. Herchel, I. Nemec and P. Neugebauer, *Dalton Trans.*, 2020, **49**, 11697-11707.